Electronic Supplementary Material (ESI) for Journal of Materials Chemistry C.

Supporting Information

Unprecedented light induced aggregation of cationic 1,4,5,8-Naphthalenediimide amphiphiles

Rafael G. Antoneli[a], Thaisa B. F. de Moraes[b,f], Helena C. Junqueira[c], Luca M. Sihn[d], Henrique E. Toma[d], Bruno Pedras[e], Luís Filipe Vieira Ferreira[e], Denis Frath[f], Christophe Bucher[f], Jonathan W. Steed[g], Gregóire J.-F. Demets[b], Eduardo R. Triboni[a]

Affiliation

[a] Laboratório Nanotecnologia e Engenharia de Processos- NEP, Universidade de São Paulo, Lorena SP, Estrada Municipal do Campinho, s/nº CEP 12.602-810, Lorena, SP, Brasil. *corresponding author: tribonier@usp.br.

[b] Departamento de Química, FFCLRP, Universidade de São Paulo, Av. Bandeirantes 3900, Ribeirão Preto SP, CEP 14040-901, Brasil.

[c]Departamento de Boquímica, Instituto de Química, Universidade de São Paulo, Butantã, São Paulo - SP, CEP 05508-000, Brasil.

[d] Departamento de Química Fundamental, Instituto de Química, Universidade de São Paulo, Butantã, São Paulo - SP, CEP 05508-000, Brasil.

[e] iBB-Institute for Bioengineering and Biosciences, Instituto Superior Técnico and Associate Laboratory i4HB - Institute for Health and Bioeconomy at Instituto Superior Técnico, Universidade de Lisboa, 1049-001 Lisboa, Portugal

[f] École Normale Supérieure de Lyon, CNRS, Laboratoire de Chimie UMR 5182, 46 allée d'Italie, 69342 Lyon, France.

[g] Department of Chemistry, Durham University, South Road, Durham DH1 3LE, UK.

S1. Characterization and Synthesis

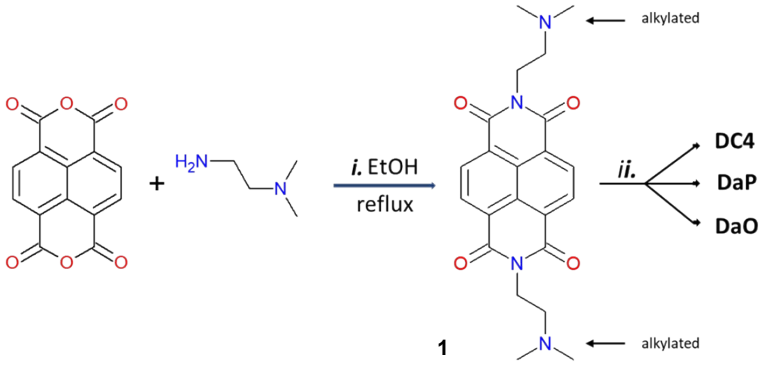

Figure S1. imidization in ethanol under reflux*; ii.* alkylation in acetonitrile for 8 h under reflux using slight excess of the alkylating agent to prepare substituted ammonium compounds **DaP**, **DaO** and **DC4**.

Imide precursor**, compound 1** - *N,N'-(N,N´-dimethylethylene)-1,4,5,8-naphthalenediimide*: ^{1}H-NMR ($CDCl_3$, ppm): 2.3 (s, 12H, N-CH_3), 2.6 (t, 4H, CH_2), 4.3 (t, 4H, N(imide)-CH_2), 8.7 (s, 4H, Ar). MS m/z (%): 408M$^+$, 377, 249, 153, 58. FTIR (KBr) n (cm^{-1}): 3078, 2821, 2771, 1700, 1663, 1450, 1349, 1243, 1070. anal. calcd. %: C 64.69, H 5.92, N 13.72; found: C 64.62, H 5.89, N 13.77.

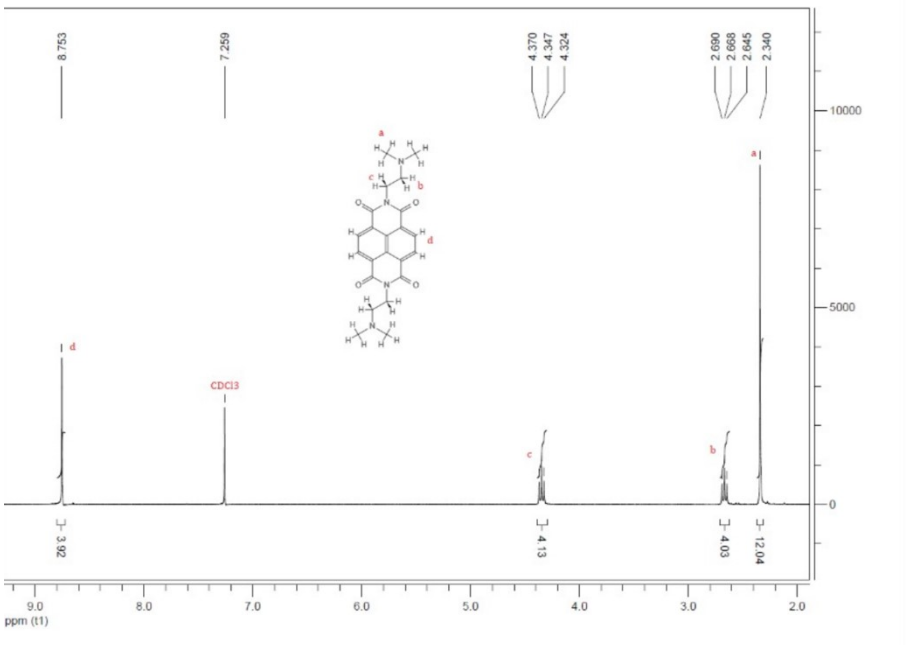

Figure S2**.** ^{1}H-NMR spectrum of imide precursor **1** (CD_3Cl 300MHz).

- DaP - *N,N'*-(*N,N*-dimethyl ethylene-*N´*-propanoic-1,4,5,8-naphthalenediimide: FTIR (KBr) ν (cm^{-1}): 3085, 2971, 1704, 1666, 1450, 1348, 1243, 1070. Elemental analysis - anal. calcd. %: C 47.07, H 4.80, N 7.84; found: C 47.01, H 4.83, N 7.79.

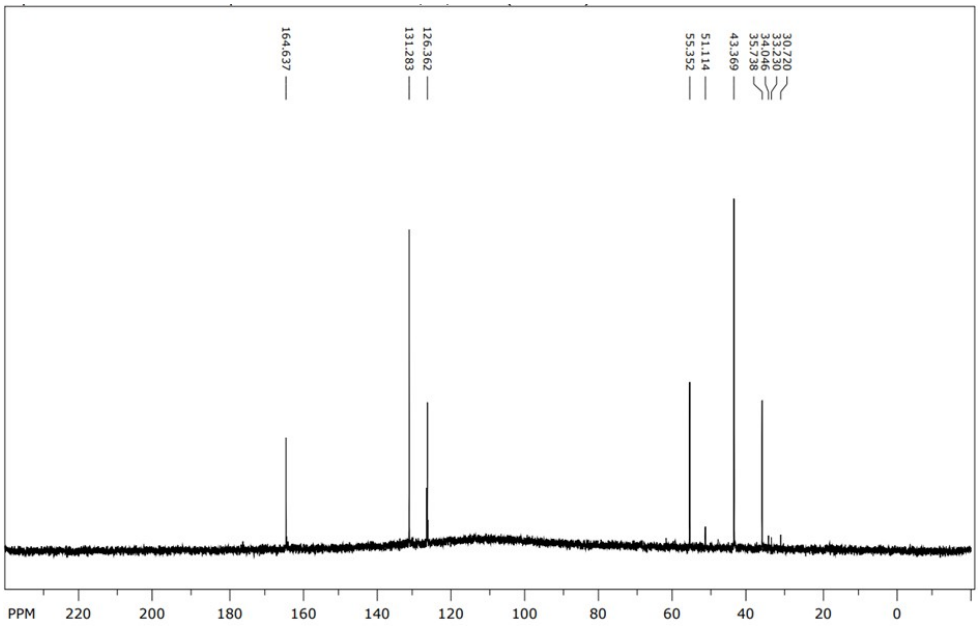

Figure S3. ^{13}C-NMR spectrum of **DaP** (D_2O 500MHz).

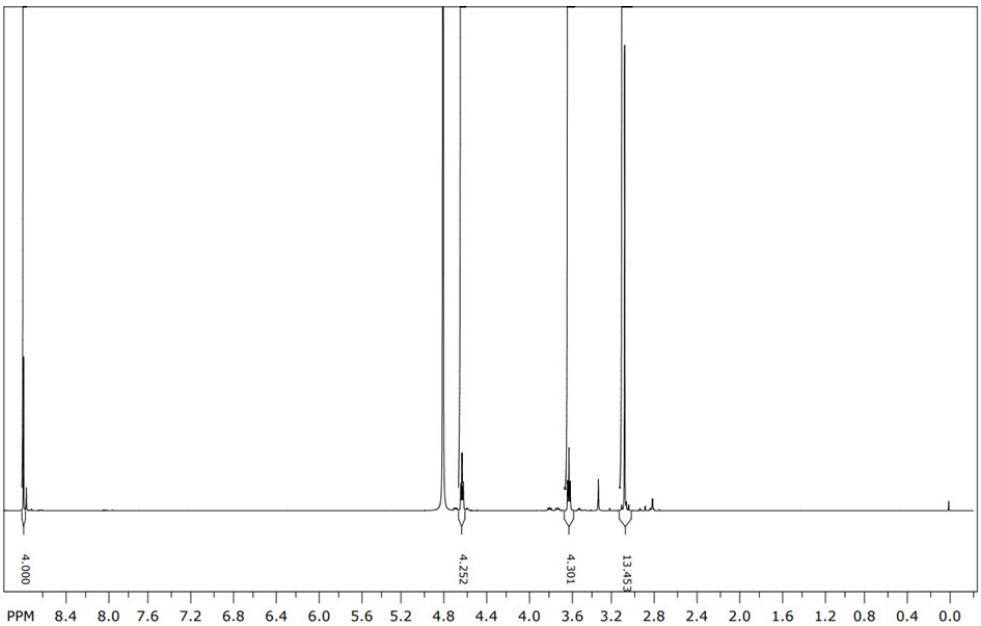

Figure S4. ^{1}H-NMR spectrum of **DaP** (D_2O 500MHz).

DaP Mass spectrum:

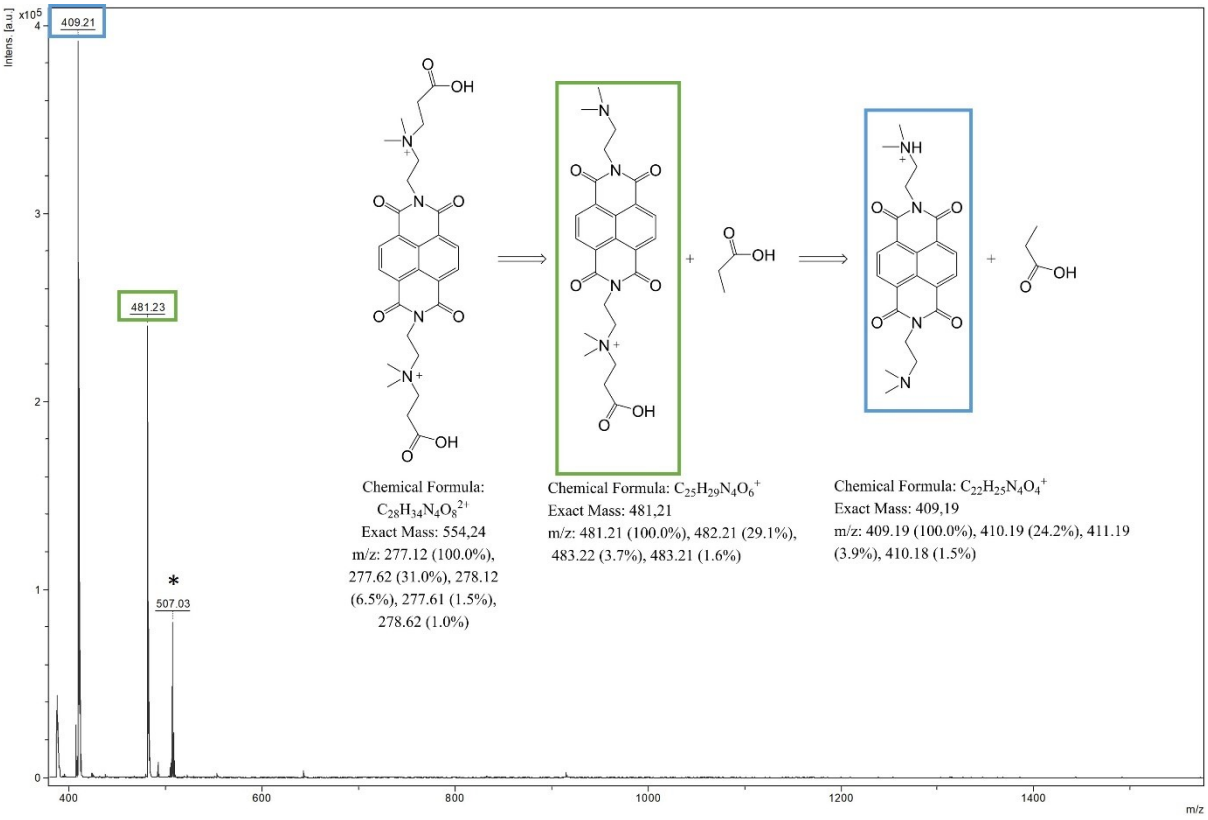

Figure S5. MALD-TOF/TOF-MS spectrum of **DaP** using DHB as a matrix. Peak assigned with (*) is attributed to DHB matrix.

- DaO - *N,N'*-(*N,N*-dimethylethylene-*N´*-octanoic)-1,4,5,8-di-naphthalenediimide. FTIR (KBr) n (cm^{-1}): 3080, 2975, 1701, 1664, 1450, 1348, 1243, 1070. Elemental analysis - calcd. %: C 53.40, H 6.37, N 6.56; found: C 53.43, H 6.32, N 8.47.

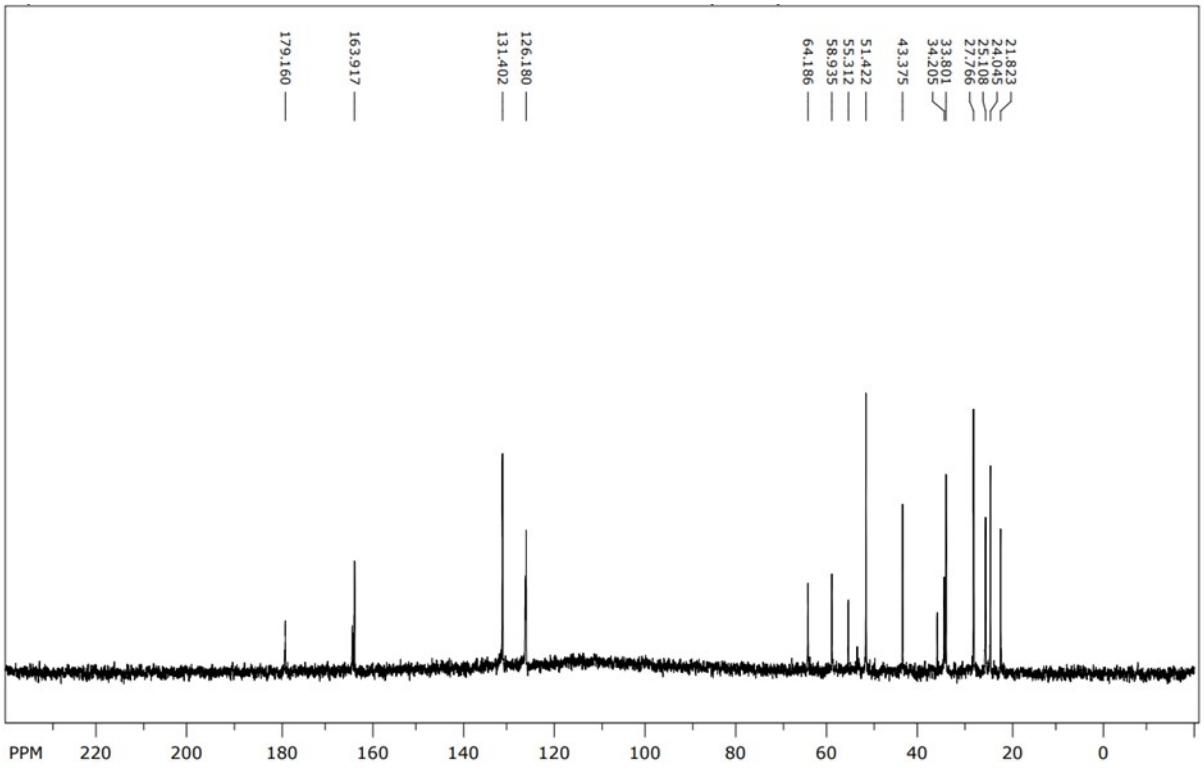

Figure S6. ^{13}C-NMR spectrum of DaO (D_2O 500MHz).

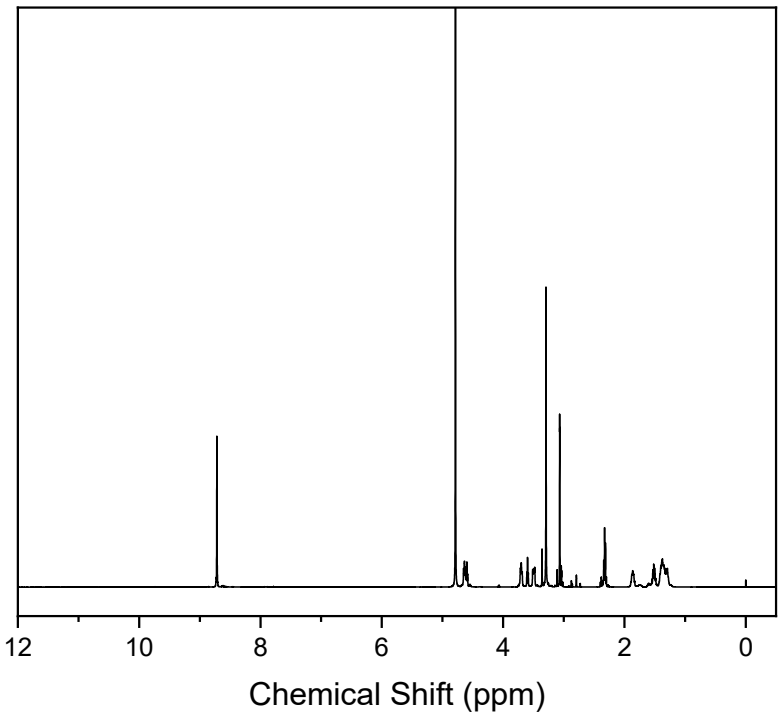

Figure S7. ^{1}H-NMR spectrum of DaO (D_2O 500MHz).

DaO Mass spectrum**:**

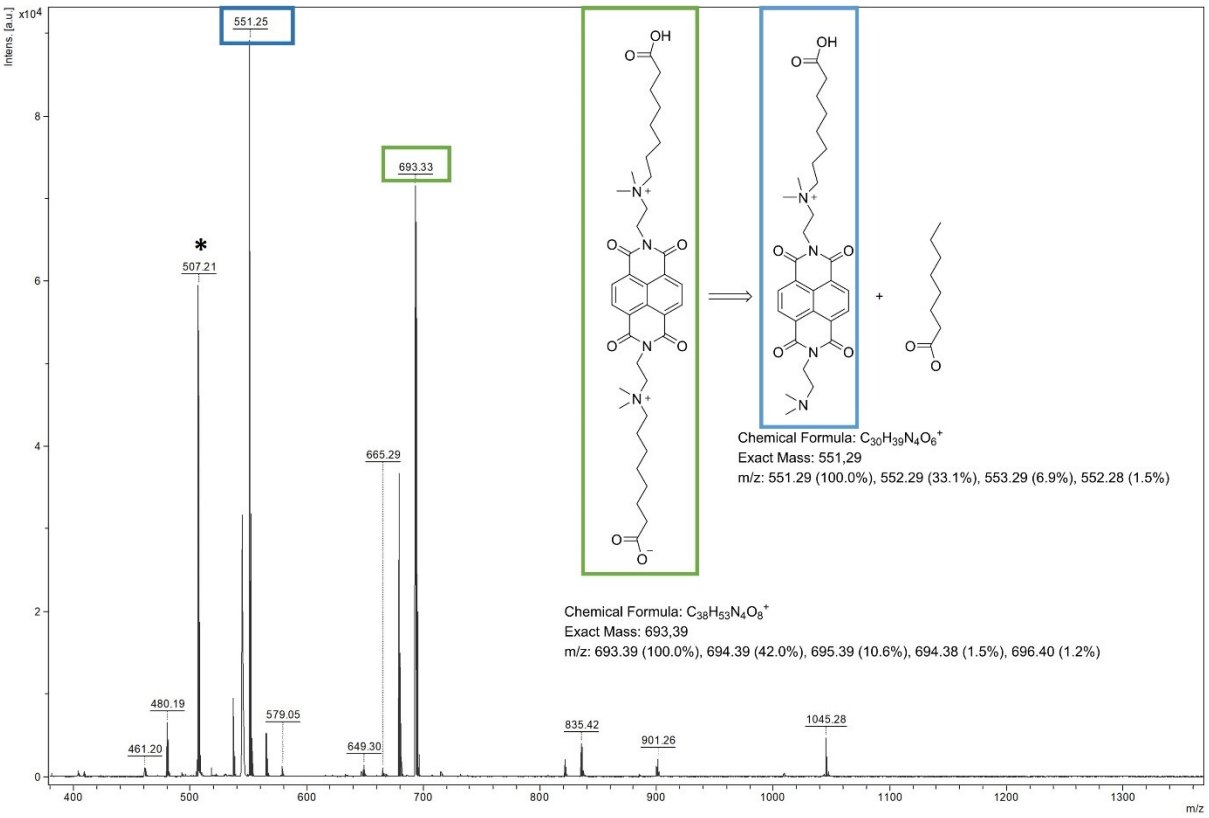

Figure S8. MALD-TOF/TOF-MS spectrum of DaO using DHB as a matrix. Peak assigned with (*) is attributed to matrix.

- DC4: *N,N'*-(*N,N*-dimethylethylene-N´-butyl)-1,4,5,8-naphthalenediimide. FTIR (KBr) ν (cm^{-1}): 2970, 2821, 1704, 1665, 1450, 1349, 1243, 1070. Elemental analysis - calcd. %: C 52.8, H 6.2, N 8.2; found: C 52.2, H 6.18, N 8.4.

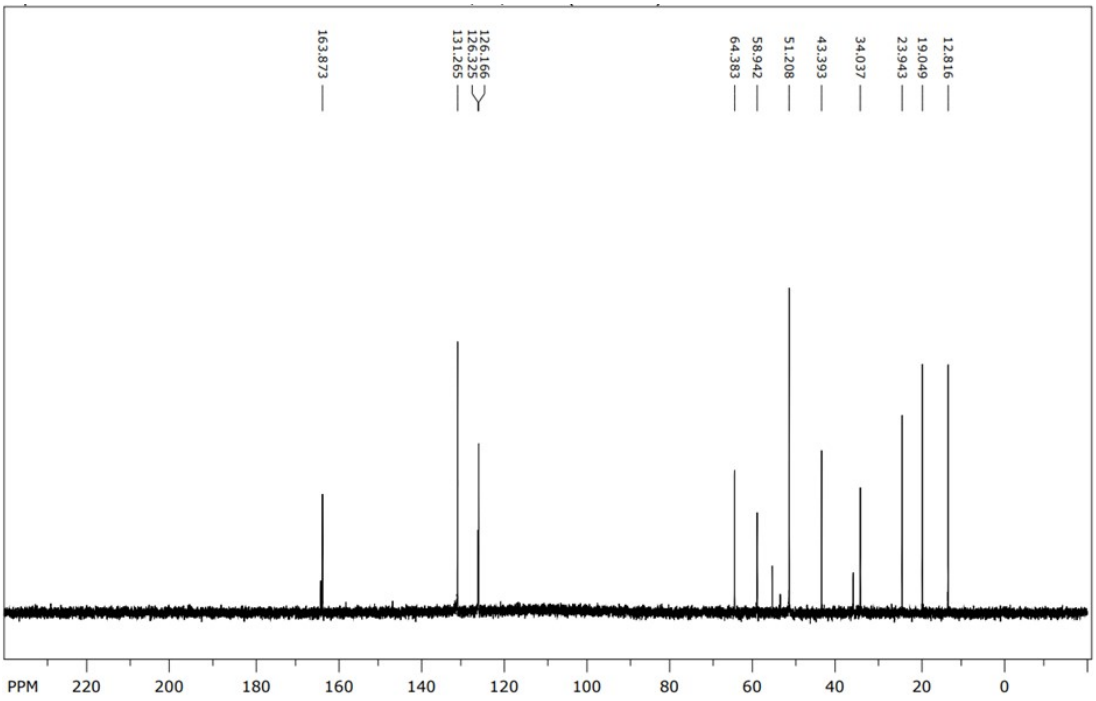

Figure S9: ^{13}C-NMR spectrum of DC4 (D_2O 500MHz).

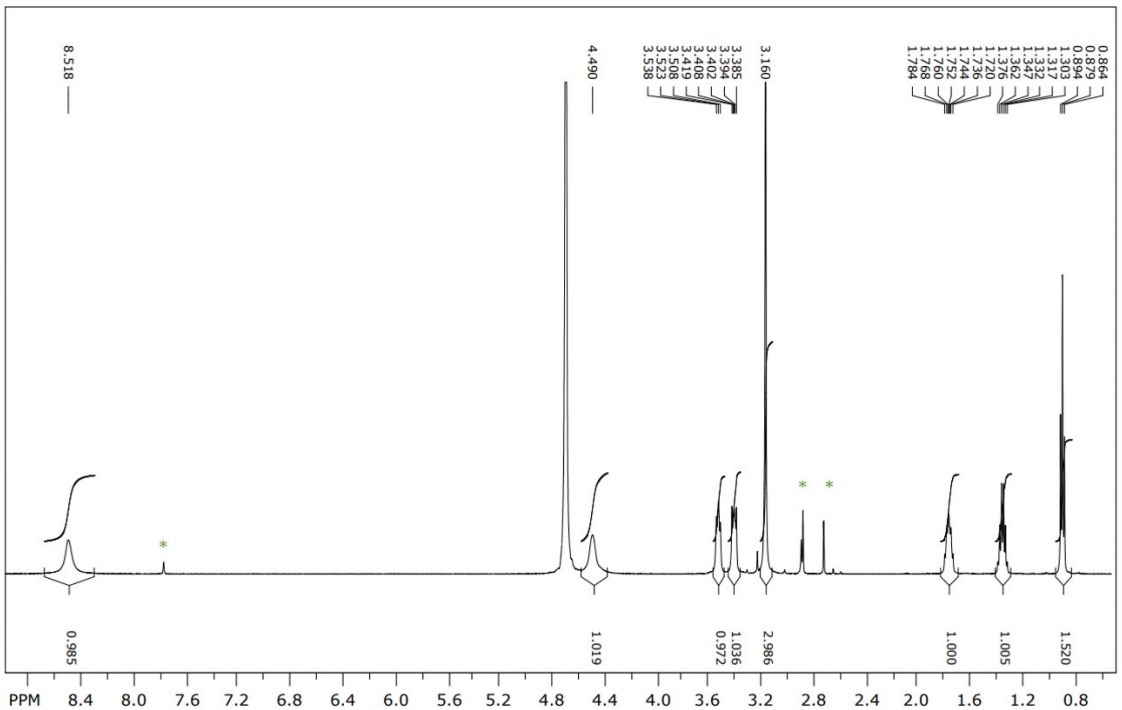

Figure S10. ^{1}H-NMR spectrum of DC4 (D_2O 500MHz). Peaks assigned with (*) are attributed to remaining Dimethylformamide (DMF).

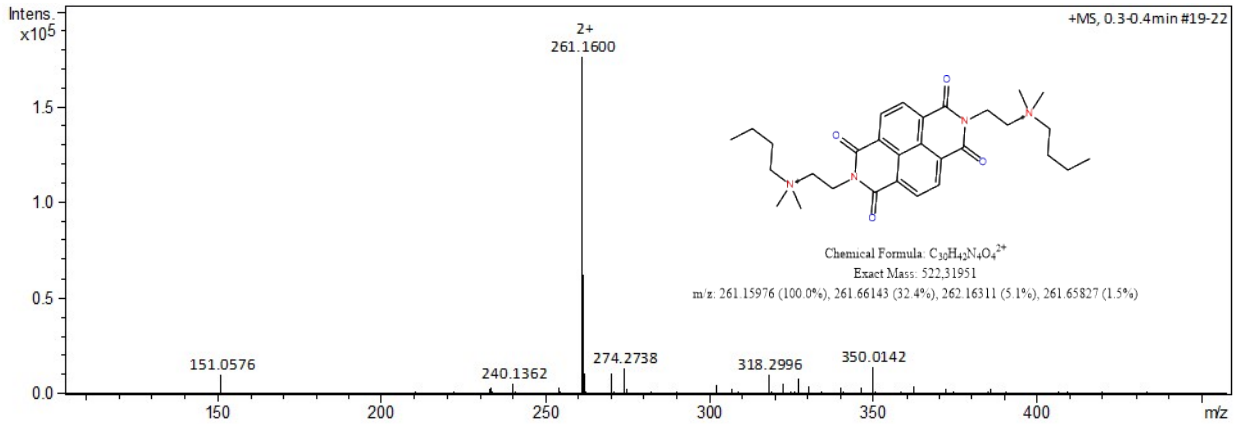

Figure S11. ESI-MS (+) of DC4 dissolved in THF and diluted with MeOH.

SI-2. UV-vis and Fluorescence

- UV-vis absorption spectra at varying concentration of the **NDI-as**:

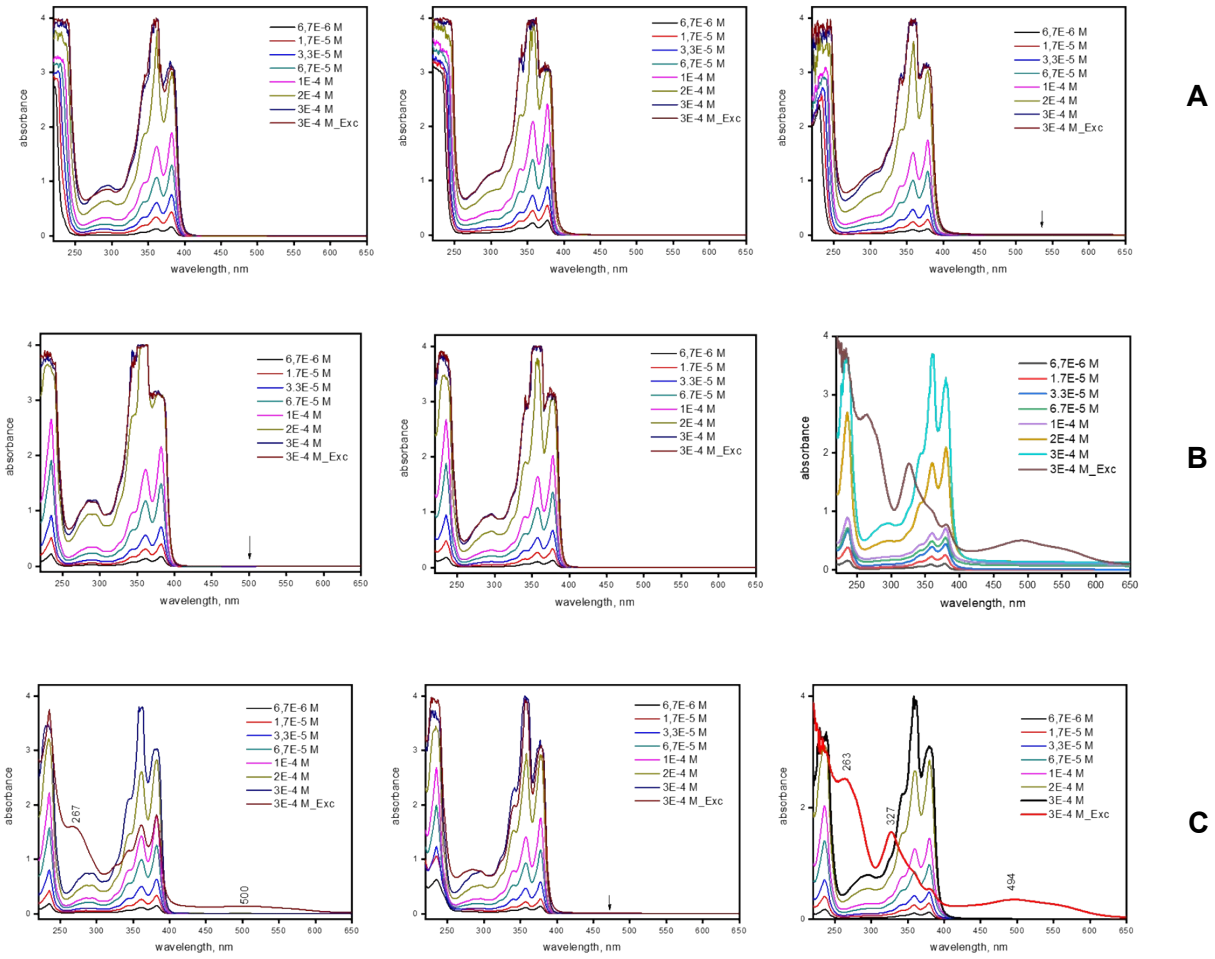

Figure S12. UV-vis absorption spectra of NDI-as over range of concentration; Left column to right: water, MeCN and THF solvents. A, B and C rows: DC4, DaP, and DaO respectively. (Exc: Light exposition: 15 min). Solution concentration below 10^{-3} M.

The concentration dependent aggregation was confirmed by showing that the absorption at 385 nm did not follow Lambert Beer law above 2.0×10^{-4}M, which is usual photophysical behaviour.

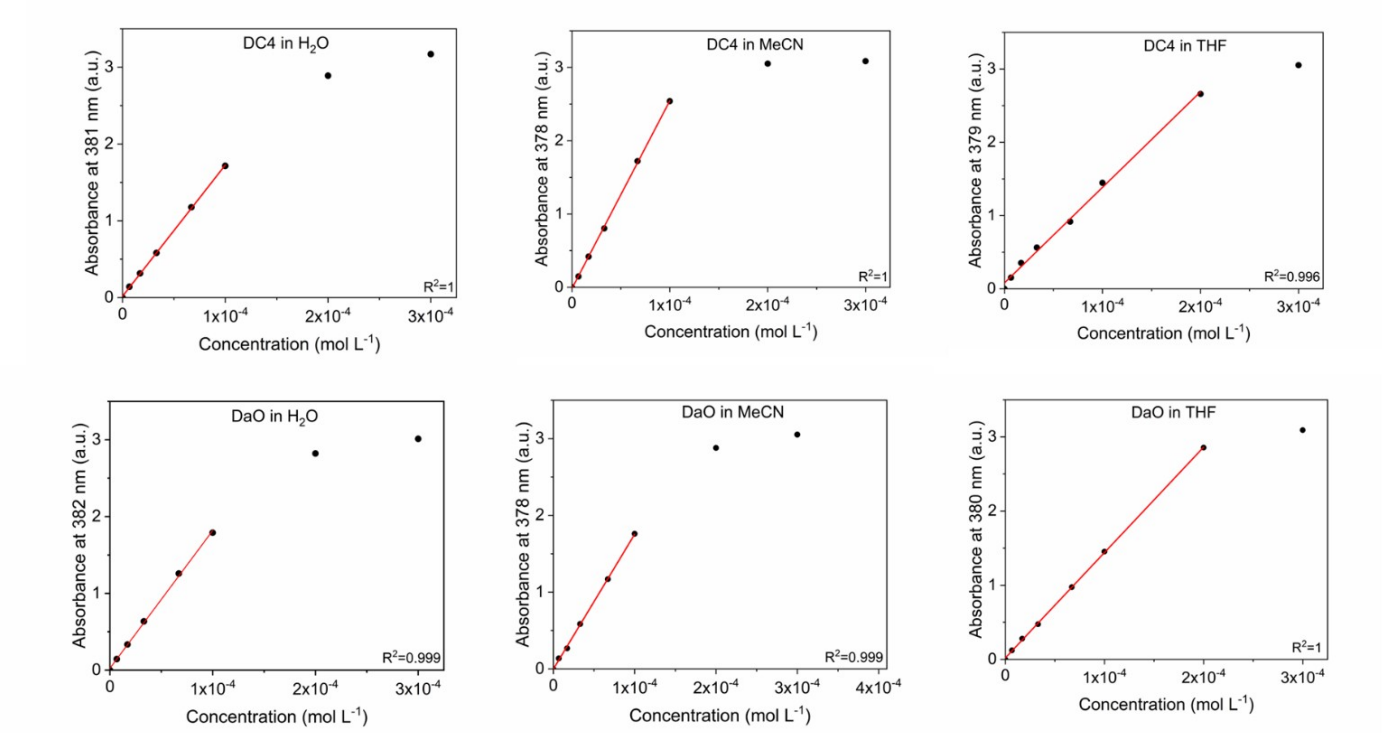

Figure S13 – Evolution of absorbance as function of concentration (optical pathway= 5 mm).

- Fluorescence spectra at varying concentration of the **NDI-as**:

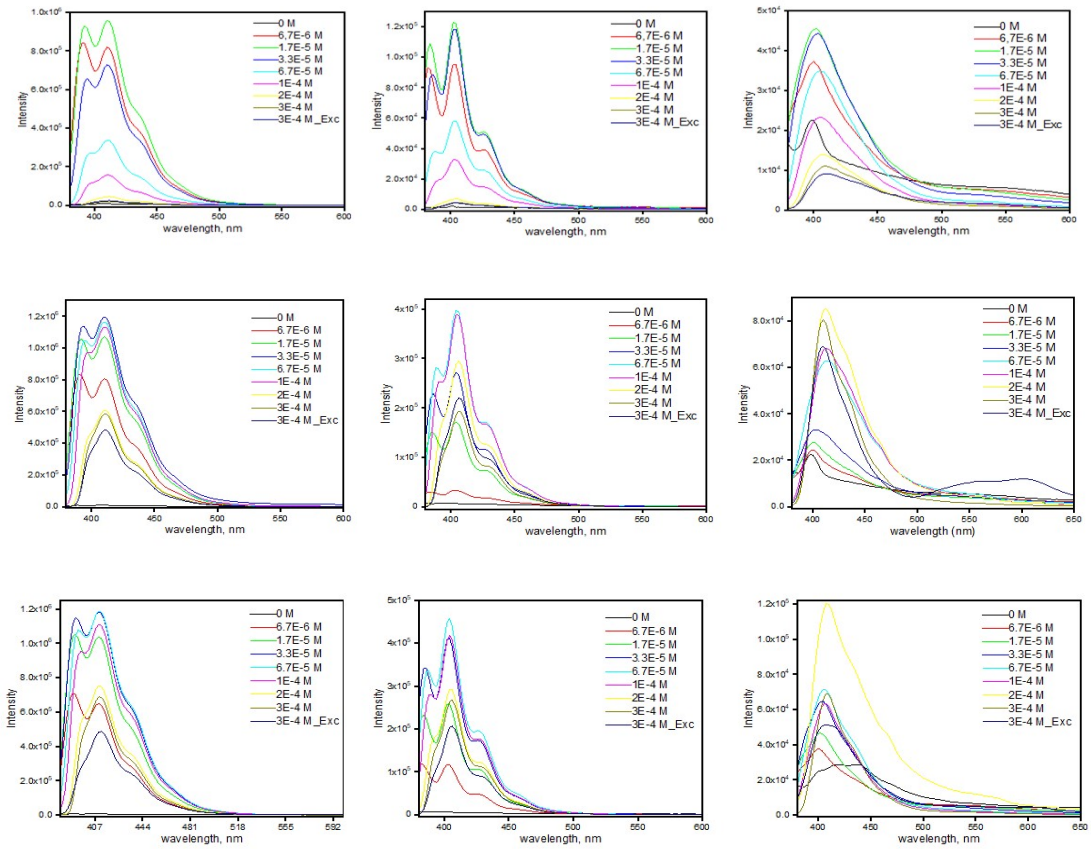

Figure S14. Fluorescence spectra of NDI-as over range of concentration; Left column to right: water, MeCN and THF solvents. A, B and C rows: DC4, DaP, and DaO respectively. (Exc: Light exposition: 15 min). Solution concentration below 10^{-3} M.

SI-3. Pictures of the quartz cuvettes upon irradiation within the fluorimeter

- Photochromism observed with light incidence:

Figure S15**.** Pictures taken at 5, 10 and 15 min irradiation of the DaO in THF, ([DaO] = 1.0x10^{-3} M).

- Absorption spectra of the **NDI-as** along light exposition time (1h):

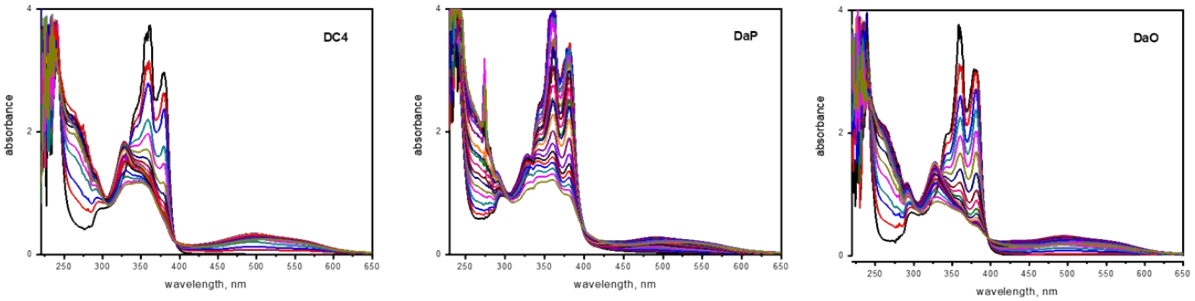

Figure S16. Samples with concentrated solutions [> 10^{-4} M] in THF.

- Excitation spectra of **DC4**, **DaP** and **DaO**:

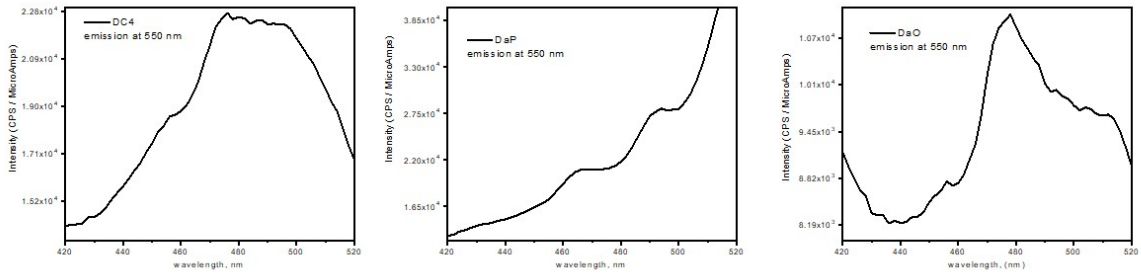

Figure S17. Emission collected at 550 nm; samples with concentrated solutions in THF (3 10^{-4}.)

- Effect of addition of $NaBF_4$:

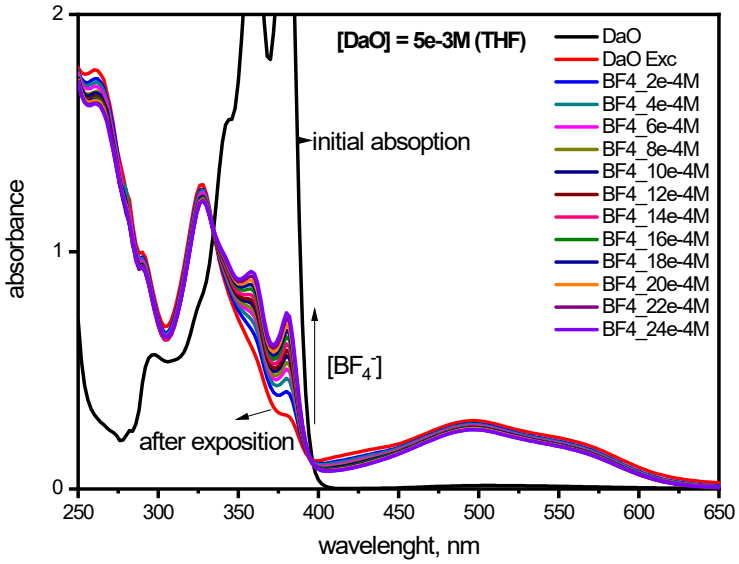

Figure S18**.** Sequential addition of the bulk salt breaks out the light-induced aggregate, refreshing the NDI vibronic peaks.

SI-4. ^{1}H-NMR integral and chemical shifts from the light/heat cycle

Table S1: Variation of the 8.72ppm signal throughout the cycle (TMS signal integral =1).

	Max. Intensity / A.U.	Integral	Chemical Shift / ppm
1	1302732.609	57	8.7183
2	10111.908	60	
3	1672301.423	61	8.7208
4	2591.807		
5	1569740.405	61	8.7225

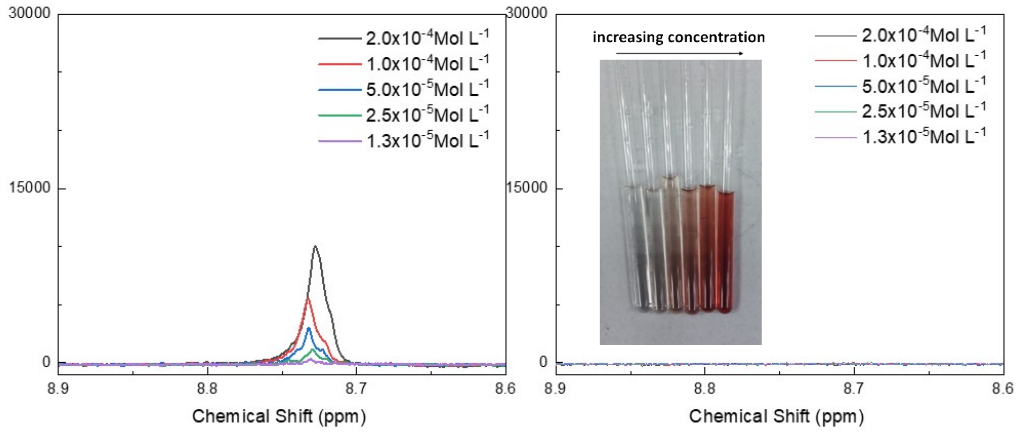

Figure S19. ^{1}H-NMR spectrum of DaO (zoom in the 8.72ppm signal) in D_2O in function of the concentration A) Before irradiation and B) after irradiation.

SI-5. Time-resolved luminescence measurements

At higher **DaO** concentration (1×10^{-4} M) in THF, fluorescence emission of the aggregate species predominates over monomer's (Fig. S20-a and -b), and phosphorescence emission is clearly observed at 77K (Fig. S20-c), whereas at room temperature, for at the same concentration, monomer fluorescence prevails (Fig. S20-d and -e) and no phosphorescence could be observed. Both monomer and aggregate emission intensities are higher at 77 K than at room temperature, which could be indicative of delayed fluorescence, provided the luminescence lifetimes at these wavelengths were comparable to the phosphorescence lifetime, which is not the case (Table S2). Further studies to investigate this behaviour will be performed. It is also noteworthy that at room temperature the fluorescence band attributed to the aggregate species appears bathochromically shifted when compared to the 77 K spectra. Both fluorescence lifetimes (monomer and aggregate) increase with as decreasing temperature, but remain within the same order of magnitude, certainly due to decrease of the non-radiative rate constants at 77 K. Aqueous solutions with the same concentration were also studied at room temperature, but the obtained luminescence intensity had a very low signal-to-noise ratio, which did not allow any determinations. Like in THF, phosphorescence was also not observed.

For more diluted **DaO** solutions (1×10^{-5} M) in THF the predominant species is the monomer, even at 77 K, as depicted in Figure S21-a and -b, and a less intense phosphorescence emission is observed when compared to the one obtained for higher **DaO** concentrations (Fig. S20-c). Nevertheless, phosphorescence lifetime in more diluted conditions is considerably higher (a more than 40-fold enhancement), which might indicate lesser non-radiative transitions due to triplet-triplet annihilation than in the more concentrated THF solution, resulting in a longer-lived excited triplet state in the former. This observation corroborates the singlet oxygen detection experiments, in which the aggregates generated more singlet oxygen than single monomers, contrarily to what is usually expected in most sensitizers. In water (Fig. S21-d and e), even at lower concentrations the predominant emission is due to the aggregate species, with a lifetime comparable to the one observed in THF. However, the fluorescence lifetime of the monomer is considerably lower than its THF solution counterpart, which points out to a higher tendency to aggregate in water than in THF. Likewise, phosphorescence lifetime in water is slightly lower than in THF for the same concentration, which is due to higher aggregation in water and, consequently, leading to higher triplet-triplet annihilation rates.

Table S2. Photoluminescence wavelength maxima and their corresponding luminescence lifetimes (t_L)* for DaO in THF and water solutions, at 293 and 77 K.

	[DaO] = 10^{-4} M		**[DaO] = 10^{-5} M**			
	λ_{em}^{max} (nm)	τ_L (THF)	λ_{em}^{max} (nm)	τ_L (THF)	λ_{em}^{max} (nm)	τ_L (H2O)
77 K	492	29 ns [(a)]	475	43.5 ns [(a)]	494	43 ns [(a)]
	412	260 ns [(b)]	401	317 ns [(b)]	410	144 ns [(b)]
	628	10 µs [(c)]	622	435 µs [(c)]	636	377 µs [(c)]
293 K	549	13 ns [(a)]	-	-	-	-
	401	216 ns [(b)]				

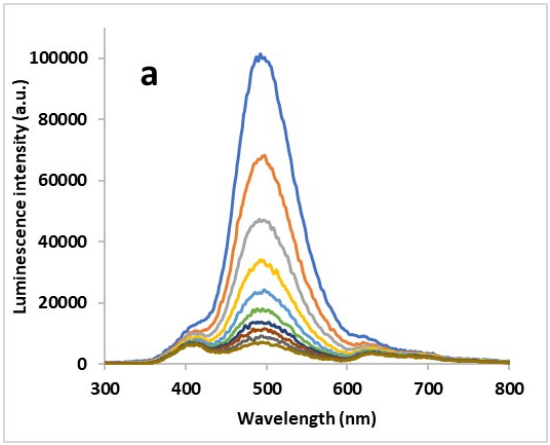

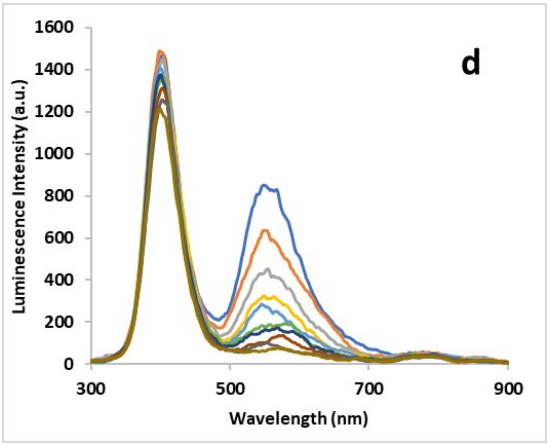

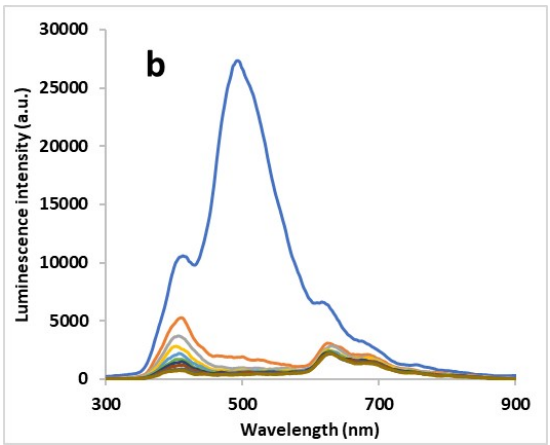

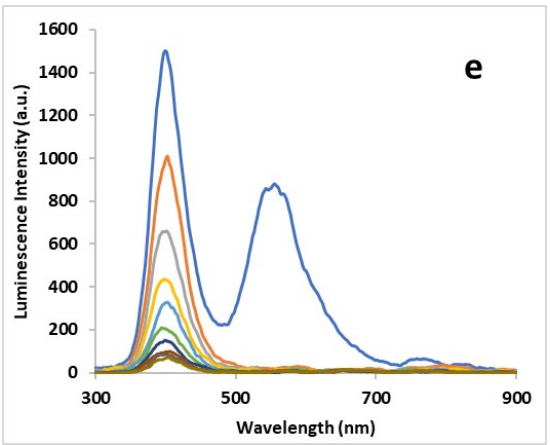

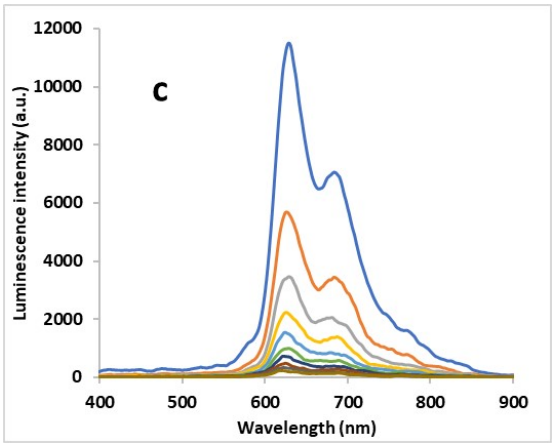

Figure S20 – Time-resolved emission spectra of **DaO** in THF solution (1×10^{-4} M), at 77 K (left) and at room temperature (*ca.* 293 K), Ar-purged (right). λ_{exc} = 337 nm (N_2 laser). All spectra were recorded with a start delay (SD) of 0 ns (blue curve) except spectrum c, with a SD of 5 μs, and increments (step) of 10 ns (a), 100 ns (b and e), 500 μs (c), 5 ns (d), with the use of gatewidths (GW) of 10 μs (a and b), 200 μs (c) and 50 μs (d and e). The luminescence intensity decreases at each delay increment.

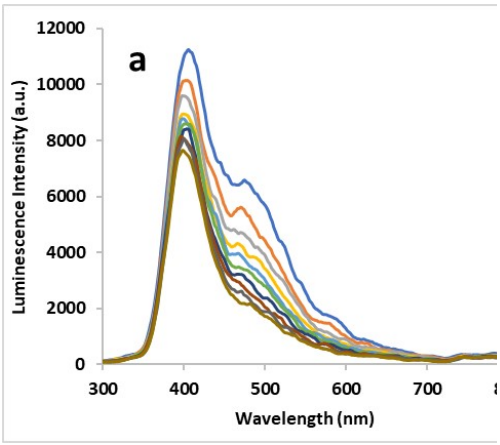

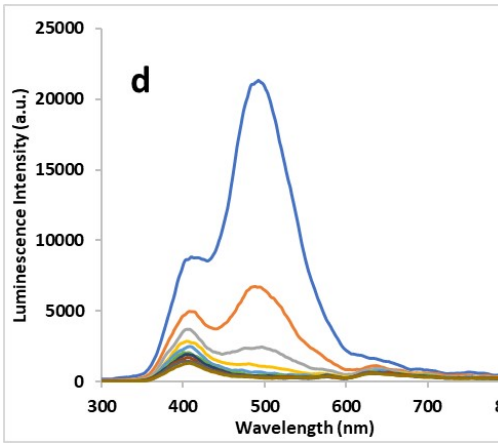

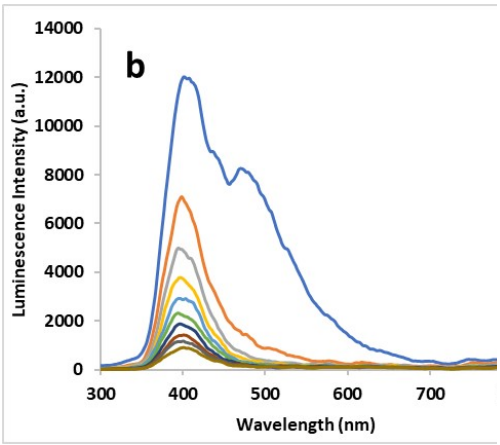

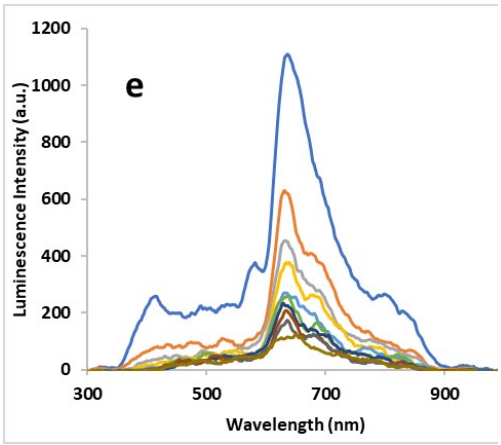

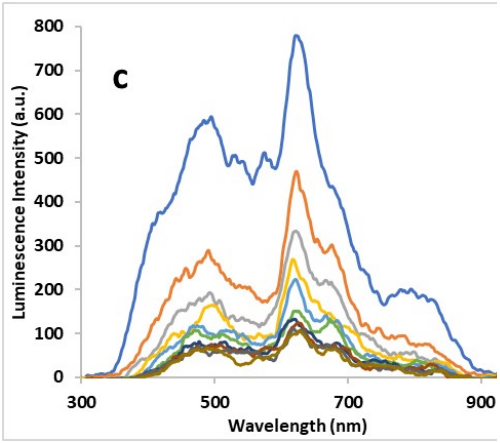

Figure S21 – Time-resolved emission spectra of **DaO** 1×10^{-5} M in THF (left) and H_2O (right), at 77 K. λ_{exc} = 337 nm (N_2 laser). Spectra a, b and d were recorded with a start delay (SD) of 0 ns (blue curve), and spectra c and e with a SD of 5 μs, and increments (step) of 5 ns (a), 100 ns (b), 100 μs (c), 50 ns (d) and 100 μs (e), with the use of gatewidths (GW) of 50 ms (a, b and d) and 200 ms (c and e). The luminescence intensity decreases at each delay increment.

Quantum Yield

The luminescence quantum yields of the DaO compound [$1.0\text{x}10^{-5}$ M] in different solvents were determined using an air-equilibrated solution of anthracene in ethanol as standard (ϕ_F = 0.21).

In aqueous media, DaO showed a higher luminescence quantum yield than in acetonitrile and THF (0.0058, 0.0027 and 0.000596, respectively). The lowest value for THF suggests a higher degree of aggregation in this solvent, in opposition to the behaviour in water, where aggregation seems to be much less pronounced.

SI-6 Electrochemical and radical generator studies

- Electrochemistry of DaO

The electrochemical characterization of the DaO was performed using cyclic voltammetry (CV) and RDE experiments. Figure S22a exhibits two reversible reduction waves assigned to the *in-situ* generation of $NDI^{\bullet-}$ and NDI^{2-}.[1] The peak current is proportional to the square root of scan rate in which follows Randles-Sevcik indicating a diffusion-controlled process (Fig S22b).[1]

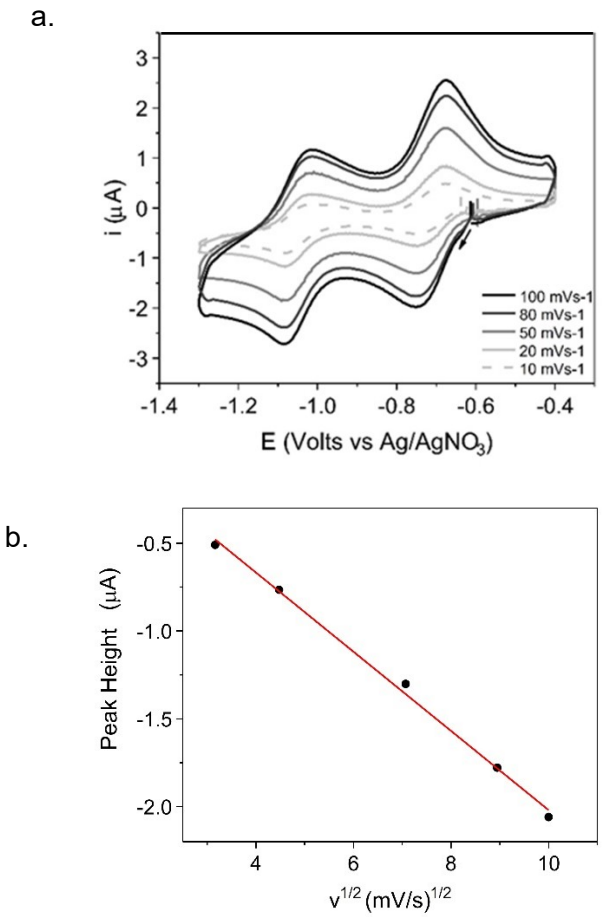

Figure S22. (a) Cyclic voltammograms of DaO in MeCN (8 10^{-5} M + 0.1 M $TBAPF_6$) ; WE: carbon; CE: Pt wire; RE: $AgNO_3$/Ag (10^{-2} M in MeCN); (b) Linear fit of the current peak height measured on the first reduction wave versus the square root of the scan rate.

Similar measurements were conducted before and after UV irradiation of 10^{-4} M DaO in MeCN (+0.1 M $TBAClO_4$). Figure S23a shows that the intensity of the reduction and oxidation peak currents decrease upon irradiation. Rotatory-disk electrode measurements also show that the decrease in the diffusion-limited cathodic current is not accompanied by an equivalent

increase on the anodic side (Fig. S23b). Those findings thus suggest that irradiation does not lead to the accumulation of reduced species in solution.

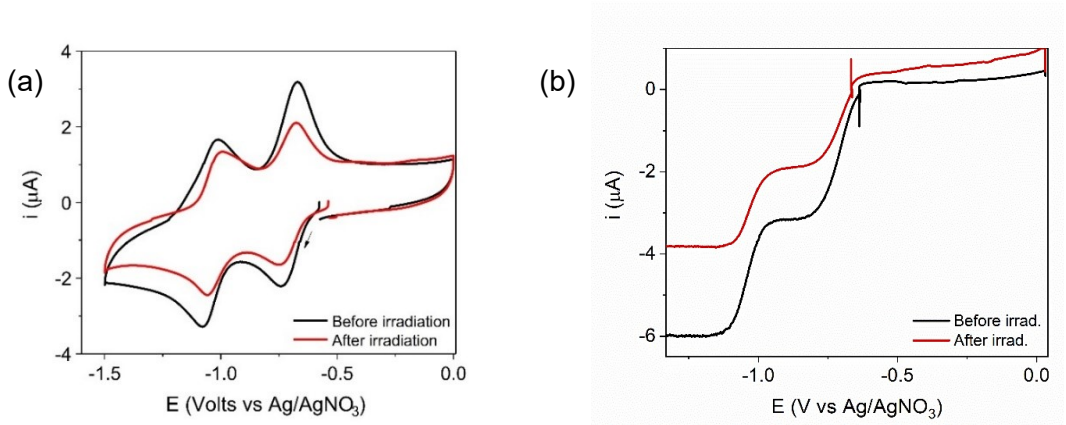

Figure S23. (a) Cyclic voltammogram of a 10^{-4} M DaO in MeCN (+ 0.1 M $TBAClO_4$) before (black line) and after (red line) irradiation at 100 mVs^{-1}; (b) Rotatory-disk electrode measurements at 500 rpm and 10 mVs^{-1}.

- Spectroelectrochemistry of DaO

Spectroelectrochemical measurements were carried out to characterize the radical anion and dianion of DaO. The radical anion ($DaO^{\bullet -}$) and (DaO^{2-}) were selectively generated in situ by exhaustive electrolysis at E_{app} = -0.85 V and -1.25 V, respectively. The absorption spectra recorded after addition of one and two electrons/molecules are shown in Figure S24. The spectrum of the $DaO^{\bullet -}$ exhibits a set of new signals at λ_{max} = 447, 473, 530, 605, 670 and 764 nm as well as a broad band in the NIR region (> 900 nm) attributed to the formation of pi-dimers (Fig. S24). [1,2] The spectrum of the $DaO^{\cdot 2-}$ exhibits intense signals centered at λ_{max} = 392, 415, 510, 551 and 597 nm, values which are in agreement with data reported for similar compounds.[1]

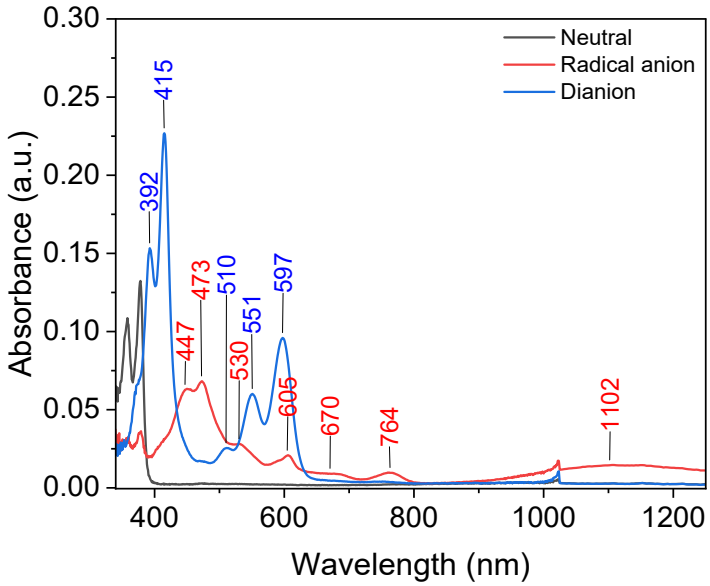

Figure S24**.** Thin-layer spectroelectrochemical data recorded before (black line) and after (red and blue lines) electrolysis of a 10^{-4} M solution of **DaO** in MeCN (0.1 M $TBAClO_4$; WE: Pt gride; CE: Pt wire and pseudo-reference electrode: Ag wire; quartz cuvette with optical pathway = 0.5 mm). The spectrum of the radical anion $DaO^{\bullet-}$ (red line) was collected after electrolysis at E_{app} = -0.85 V. The spectrum of the dianion DaO^{2-} (blued line) was collected after electrolysis at E_{app} = -1.25 V.

- Influence of radical anion on the self-assembly of DaO

DaO was reduced chemically by progressive addition of Tetrakis(dimethylamino)ethylene (TDAE) to a 10^{-4} M solution of DaO in acetonitrile (Fig. S25a). The in-situ formation of the radical anion $DaO^{\bullet-}$ was followed by UV-vis spectroscopy measurements. The spectra recorded after addition of 0.1, 0.3 and 0.5 molar equivalents of TDAE are shown in Figure S25b. As observed on the spectroelectrochemistry data discussed above, the formation of $DaO^{\bullet-}$ is revealed by the development of bands at λ_{max} = 453, 474, 529, 608, 677, 758 nm coming along with a decrease in the intensity of the bands attributed to DaO at 340, 358 and 378 nm. (Fig. S24), the colour of the solution changing from colorless to brownish (Fig. S25a). Then, the solution of $DaO^{\bullet-}$ was exposed to oxygen to trigger its re-oxidation into DaO (Fig. S25c). The initial UV-vis spectrum (colorless) of DaO was completely recovered after 20 min under air. No evidence of self-assembly could be observed during these experiments.

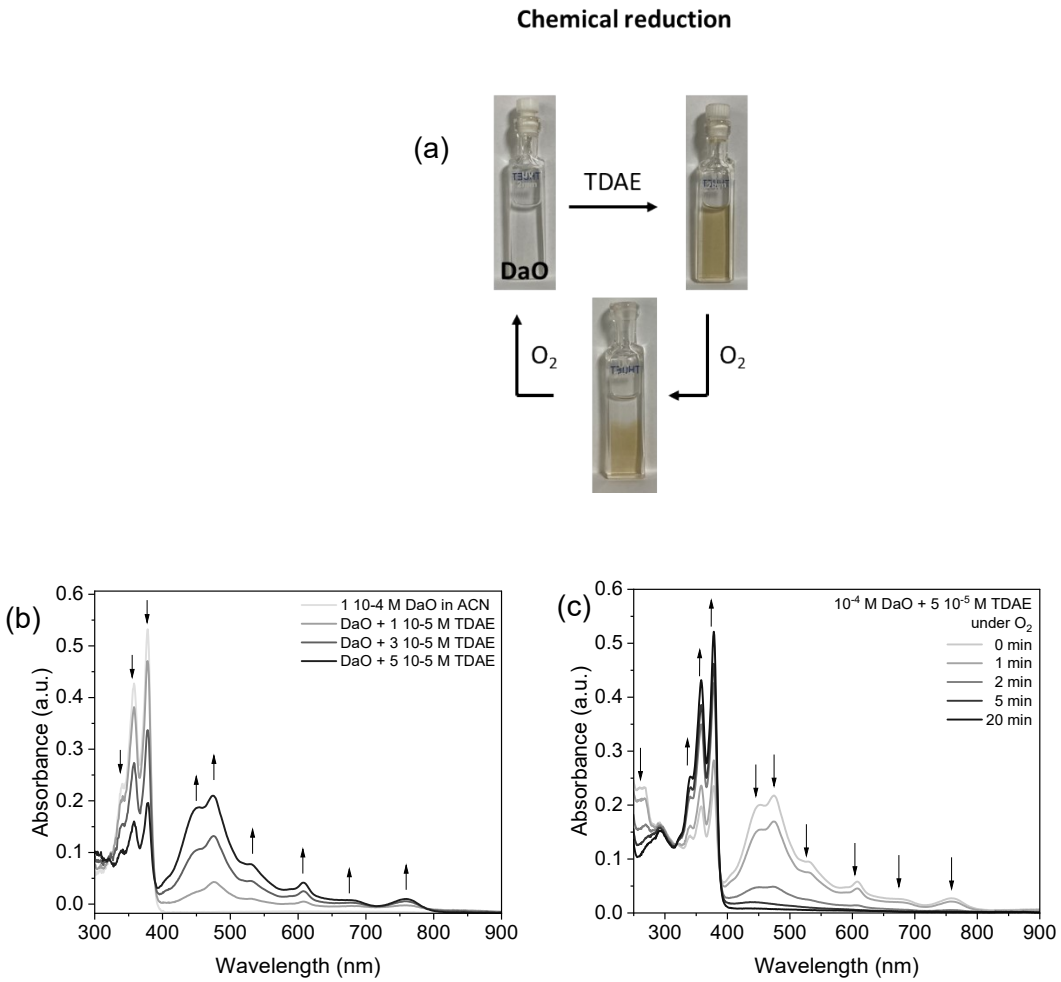

Figure S25. (a) Reversible color change observed after chemical reduction of DaO with TDAE and re-oxidation with O_2; (b) Evolution of the UV-vis absorption spectra after addition of TDAE to a 10^{-4} M solution of DaO in MeCN under argon; (c) UV-vis absorption spectra recorded after exposure of the solution to air. (optical pathway= 2 mm, Room temperature)

SI-7. Singlet oxygen measurements

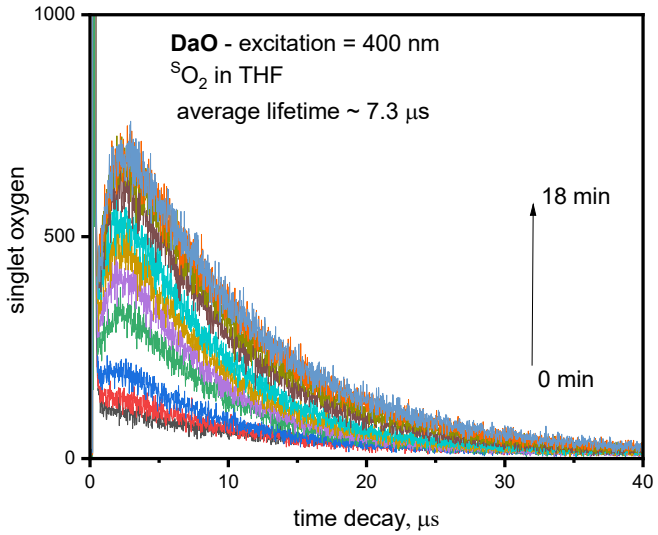

Figure S26**.** Singlet oxygen generation during the irradiation period (18 min) when exciting **DaO** at 400 nm.

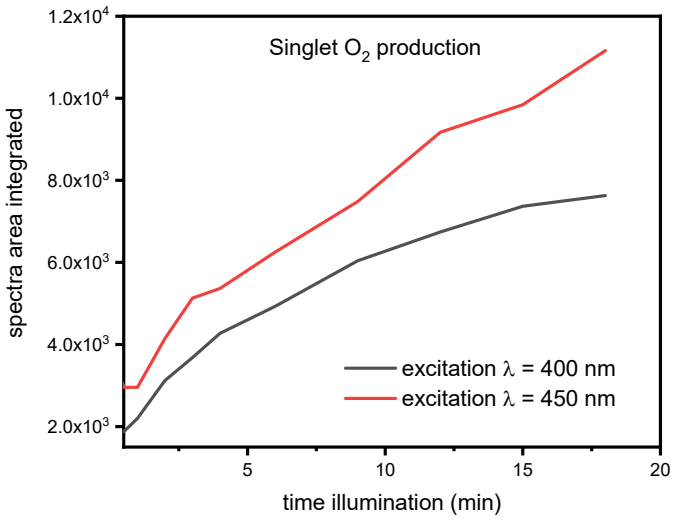

Figure S27. Comparison between O_2 singlet generation using two different excitation wavelengths (400 or 450 nm).

References

[1] Andric, Goja, et al. "Spectroscopy of naphthalene diimides and their anion radicals." *Australian Journal of Chemistry* 57.10 (2004): 1011-1019.

[2] Takai, Atsuro, et al. "A Directly Linked Ferrocene–Naphthalenediimide Conjugate: Precise Control of Stacking Structures of π-Systems by Redox Stimuli." *Angewandte Chemie International Edition* 52.35 (2013): 9167-9171.